OBTAINING ACTIVATED BIOCHAR FROM OLIVE STONE USING A BENCH SCALE HIGH-PRESSURE THERMOBALANCE

M. Puig-Gamero, A. Esteban-Arranz, L. Sanchez- Silva[*], P. Sánchez

Department of Chemical Engineering, University of Castilla –La Mancha Avda. Camilo José Cela 12, 13071 Ciudad Real, Spain

*Corresponding author phone: +34 926 29 53 00 ext. 6307; fax: +34 926 29 52 56;

e-mail: marialuz.sanchez@uclm.es

Abstract

A low cost-biomass, olive stone, was used as a carbon precursor to synthesise activated biochar. Experiments were carried by single step activation for two agents (steam and CO_2) using a bench scale high-pressure thermobalance. Temperature, pressure, flow rate and holding time were optimised according to the highest adsorption capacity of the biochar obtained. In this respect, activation conditions were established at 900 ºC for 30 min, at 0.15 ml/min and 1 bar for H_2O activation. The optimum activation conditions for CO_2 activation was found to be 1000 ºC for 30 min, at 300 mL/min and 1 bar. The activated biochars yielded were characterised by adsorption-desorption of N_2 at -196 ºC, scanning electron microscopy, Raman spectroscopy, thermogravimetric analyses and elemental analyses. Results showed that the CO_2 activation only generated microporosity developed in the biochar, whereas both meso and micropores were created after steam activation. Then, the optimum materials were evaluated as a possible CO_2 adsorbent and for this purpose, the CO_2 adsorption isotherms over the pressure range of 1-20 bar at 30 ºC were studied. Moreover, the results for these isotherms results were fitted to Langmuir, Freundlich and Sips isotherm models, and the latter forecast the results most accurately.

Keywords: olive stone, physical activation, CO_2 uptake, activated biochar, porosity

1. Introduction

Adsorption is thought to be one of the most potential and effective alternatives for removing a wide variety of organic and inorganic pollutants dissolved in aqueous media or for gas purification [1]. Regenerating the adsorbent is easier and cheaper in comparison to other applications [2]. However, selecting a good one is still crucial (which ideally must be available, low cost, highly resistant, environmentally friendly, display high adsorption capacity and selectivity under operating conditions and have easy regeneration capacity). Among the different solid adsorbents (zeolites, MOFs…), carbon-based materials, activated carbons in particular, are the most used materials for treating wastewater and emissions [3, 4], since they have well-developed porosity which provides high adsorptive capacity per volume unit and great selectivity for gases and organic vapours. Heretofore, anthracite and bituminous coals were the main sources of activated carbon. However, these materials can be generated from any carbonaceous source [3] and in this regard, activated biochars from agro-industry biomass is an interesting and optimal choice, of great interest in the last decade. In addition, one advantage of these materials is they capture atmospheric carbon when growing, thereby reducing the carbon footprint of the final material [5]. Another important benefit of activated biochars derived from biomass sources (as opposed to traditional ones) are their high availability and low cost of production [6]. For that reason, several researchers have been focused on industrial and agricultural wastes or by-products for activated biochars synthesis. These include shells, stones and seed of fruits (almond shells, hazelnut shells, poplars, walnut sawdust [7, 8], orange peel [9], cherry stones[10], date seeds [11]) and wastes resulting from the production of cereals, bagasse (rice husks [12, 13], sugarcane bagasse [14], tea leaves [8, 13]). Other lignocellulosic sources include paper mill sludge [14].

Now, focusing on Spanish agro-industrial biomass, there are several reasons why olive stone is a good candidate as a raw material for obtaining activated biochars. Firstly, high availability since Spain is the primary producer and exporter of olive oil in Europe [15] and it has a high amount of fixed and elemental carbon content [3]. In addition, its low ash content means it efficient for producing microporous activated carbons [10].

Producing activated biochars from olive stone precursors may involve physical or chemical activation. The former consists in partial gasification in a CO_2 or steam atmosphere [16, 17] among other gases, while in the latter, chemical activators such as KOH, H_3PO_4, and $ZnCl_2$ are required [18, 19]. In this paper, physical activation was selected due to lower energy consumption and processing time, which means a lower production cost and environmental impact than in chemical activation. Normally, physical activation is carried out in two steps: carbonization and activation. In this regard, Peredo-Mancilla et al., (2018) studied the effect of different activation methods for producing activated biochars from olive stone for CO_2 capture. They concluded that physical activation favoured CO_2 adsorption capacity [20]. Plaza et al., (2019) designed a novel multibed heat-integrated vacuum and temperature swing adsorption process to capture CO_2 emitted from a coal-fired power plant. They captured around 60% of total CO_2, and concluded that this value was insufficient for reaching climate change targets , and thus, the adsorbent characteristics needed enhancing [21]. Conversely, single-step production consists in simultaneous carbonisation and activation, like gasification. Some benefits are energy saving, and require less time. Additionally, it is easier to control the physicochemical properties of the adsorbents than in two-step activation [22]. However, few studies have been reported on single-step activation. Hence, the aim of this paper was to optimise synthesis of different activated biochars by combining the carbonisation and

physical activation processes in a single step, using a bench scale high pressure thermobalance (LINSEIS STA HP/2 HP-TGA DSC). This equipment is a novel technique and useful tool for obtaining information on mass loss or mass gain during biomass conversion, which helps to obtain an accurate value for burn-off and carbon yield. Another benefit to this technique is biochar can be evaluated as a possible CO2 adsorbent in a single step at different pressures. In addition, initial sample weight, temperature and pressure can be higher than those used in conventional laboratory equipment. Therefore, the results obtained from this bench plant device can provide more valuable and realistic information for simulating industrial conditions.

As far as we know, few studies have been published on the effect of experimental conditions (especially pressure) on activated biochar production in a single-step process on a bench scale. Therefore, a thorough study on how different activation conditions (temperature, pressure, activating agent (steam and CO_2), flow rate and holding time) affects the degree of burn-off, CO_2 adsorption capacity and the physicochemical properties of the activated biochars produced on a bench scale was carried out. Finally, the most promising activated biochar materials were tested as possible CO_2 adsorbents. Then, their adsorption results were compared to those obtained from commercially activated carbon material to gain information for using these materials in a real industrial setting.

2. Materials and methods

2.1. Materials

In this paper, olive stone (Os), obtained from "*Aceites Garcia de la Cruz*" olive oil mill, Madridejos (Toledo, Spain), was used as precursor for producing activated biochar. Note that the olive stone was not milled or dried, since these specifications were adequate to use directly, reducing the operational costs. The particle size between 2 and 4 mm was

selected. While the commercial activated carbon was purchased from Sigma Aldrich (850 m^2/g). The ultimate and proximate analyses, which were performed according to UNE standards 15104:2011, UNE–EN ISO18123, UNE 32-004-84 and UNE 32002-95, can be seen in Table 1.

Table 1. Ultimate analysis and proximate analysis of the olive stone.

Proximate analysis (wt. %) *daf			
Moisture	Ash	Volatile matter	Fixed carbon *diff
7.91	1.95	69.25	20.89

Ultimate analysis (wt. %) *daf				
C	H	N	O *diff	S
49.88	6.12	nd	44.00	nd

*daf: dry and ash free basis; O*diff: % of oxygen calculated from differences in C, H, N and S; Fixed carbon*diff: % of fixed carbon was calculated from differences in moisture, ash and volatile matter; and nd: non detectable.

2.2. Single-step activation with CO_2 or steam

In this research, single-step physical activation with carbon dioxide or steam was carried out in a High Pressure (HP) thermobalance (LINSEIS STA HP/2 HP-TGA DSC). The schematic and detailed description of the system can be found elsewhere [23]. During carbonisation, the olive stone was heated from room temperature to 600 ºC at a heating rate of 10 ºC/min under a constant N_2 flow of 300 Nml/min. Then, it was kept at this temperature for 60 min. Finally, the resulting char was heated to the desired activation temperature at a heating rate of 20 ºC/min in a constant N_2 atmosphere. Subsequently, the activation agent was fed under selected conditions to start biochar activation immediately. At this point, activation agent (CO_2 or H_2O), temperature (700-1100 ºC), holding time (15-60 min), flow (300-900 Nml/min for CO_2 and 0.07-0.3 ml/min for H_2O)

and pressure (1-10 bar) were all varied to evaluate their effect on CO_2 uptake and were optimised. In this respect, the synthesised activated biochars were designated according to the following sequence: activation agent-temperature-holding time-flow rate-pressure. As a result, activated biochar produced in a H_2O atmosphere at 1000 ºC and kept at this temperature for 30 min at a flow rate of 0.3 ml/min and at atmospheric pressure was named H_2O-1000-30-0.3-1. Table 2 shows the operating conditions for each sample and the names used to identify them.

Table 2. Operating conditions used in the different activated biochar synthesised.

Sample	Activation agent	Temperature (ºC)	Holding time (min)	Flow rate (mL/min)	Pressure (bar)
H_2O-700-30-0.3-1	H_2O	700	30	0.3	1
H_2O-800-30-0.3-1	H_2O	800	30	0.3	1
H_2O-900-30-0.3-1	H_2O	900	30	0.3	1
H_2O-900-15-0.3-1	H_2O	900	15	0.3	1
H_2O-900-30-0.3-1	H_2O	900	30	0.3	1
H_2O-900-60-0.3-1	H_2O	900	60	0.3	1
H_2O-900-30-0.07-1	H_2O	900	30	0.07	1
H_2O-900-30-0.15-1	H_2O	900	30	0.15	1
H_2O-900-30-0.3-1	H_2O	900	30	0.3	1
H_2O-900-30-0.15-1	H_2O	900	30	0.15	1
H_2O-900-30-0.15-10	H_2O	900	30	0.15	10
CO_2-700-60-300-1	CO_2	700	60	300	1
CO_2-800-60-300-1	CO_2	800	60	300	1
CO_2-900-30-300-1	CO_2	900	30	300	1
CO_2-1000-30-300-1	CO_2	1000	30	300	1
CO_2-1100-30-300-1	CO_2	1100	30	300	1
CO_2-1000-15-300-1	CO_2	1000	15	300	1
CO_2-1000-30-300-1	CO_2	1000	30	300	1
CO_2-1000-60-300-1	CO_2	1000	60	300	1
CO_2-1000-30-300-1	CO_2	1000	30	300	1
CO_2-1000-30-600-1	CO_2	1000	30	600	1
CO_2-1000-30-900-1	CO_2	1000	30	900	1
CO_2-1000-30-300-1	CO_2	1000	30	300	1
CO_2-1000-30-300-10	CO_2	1000	30	300	10

2.2. Characterization of materials

The activated biochar yield was calculated by dividing the mass of the activated biochar produced by the initial mass of the dried precursor and activation burn-off was calculated as follows:

$$Burn-off \ (\%) \ = \ \frac{w_o - w_f}{w_o} \qquad (1)$$

where w_o and w_f (wt.%) are biochar mass before and after activation, respectively.

Texture properties such as: specific surface area, pore volume and pore size of the biochars were assessed by N_2 adsorption-desorption isotherm analyses at -196 ºC using a volumetric adsorption analyser (ASAP 2010 Micromeritics system). Prior to each measurement, the samples were degassed in a vacuum at a temperature of 180 ºC for 5h. Specific surface area was calculated using the Brunauer Emmett Teller (BET) method. Average pore volume and average pore diameter were calculated using the Dubinin-Radushkevich equation with N_2 adsorption-desorption data. The morphology of the biochar samples was assessed using high resolution scanning electron microscopy (HRSEM) (GeminiSEM 500). Raman spectra were recorded by a SENTERRA spectrophotometer using an excitation wavelength of 532 nm. The spectra shown are the result of 5 measurements per sample. Thermal degradation of biochar samples was assessed with a Thermogravimetric analyser (TGA-DSC 1, METTLER TOLEDO) in an air atmosphere (100 ml/min) at a heating rate of 10 ºC/min from room temperature to 1000 ºC. The ultimate analysis was determined according to the aforesaid UNE standards, and the Van Krevelen diagram (H/C vs O/C ratios) was calculated and shown.

2.3 CO_2 adsorption isotherms

CO$_2$ adsorption isotherms at 30 ºC and up to 20 bar were performed with a high-pressure thermobalance (LINSEIS STA HP/2 HP-TGA DSC) until a constant mass was reached. The equilibrium criterion was set to a maximum of 0.05 wt.% change over 10 min. The initial mass of the sample used for the adsorption isotherms depended on the activated biochar yield obtained during activation, which was between 0.1 and 0.5g. Prior to adsorption, the sample was dried in situ at 105 ºC for 30 min. Then, it was cooled to the measuring temperature, and subsequently, the system was pressurized.

Adsorption isotherm models have been widely used to predict the behaviour and maximum adsorption capacity of a material over a wide range of temperatures and pressure. In this paper, three empirical models were selected to fit the CO$_2$ adsorption isotherm data: Langmuir, Freundlich and Sips standard isotherm models. The first assumes that adsorption takes place at specific energetically homogeneous sites. In addition, a dynamic equilibrium is considered between adsorbed and non-adsorbed molecules as well as the formation of a single layer of molecules at a constant temperature and pressure. The Langmuir equation is described below as [24]:

$$q = \frac{q_e b P}{1 + bP} \tag{2}$$

where q (mmol/g) is the adsorbed quantity, P is the equilibrium pressure of the gas adsorbed (bar), q$_e$ is the maximum single-layer adsorption capacity and b is the affinity constant or Langmuir constant related to the apparent energy of adsorption. It indicates how strong an adsorbate molecule is attracted to a surface.

The Freundlich isotherm is an empirical equation that assumes adsorption on heterogeneous surfaces with interaction between adsorbed molecules as well as multilayer adsorption. The Freundlich model can be expressed by the following equation [25]:

$$q = K_F P^{1/n} \tag{3}$$

where K_F is the Freundlich isotherm constant (mmol g^{-1} bar$^{-1/n}$) and n is the heterogeneity factor or Freundlich coefficient that represents deviation from the linearity of adsorption. 1/n is the Freundlich intensity parameter, and values under 1 represent favourable adsorption [26].

Sips is a semi-empirical model and combines the Freundlich and Langmuir models, representing systems where a single adsorbed molecule could fill more than one adsorption site. This model was developed for forecasting heterogeneous adsorption systems. At low adsorbate pressures, it is reduced to the Freundlich model, while at high pressures, it predicts single-layer adsorption capacity, a feature of the Langmuir isotherm. The Sips isotherm equation can be expressed as follows [27]:

$$q = \frac{q_e(K_s P)^{1/n}}{1 + (K_s P)^{1/n}} \tag{4}$$

where q (mmol g^{-1}) is the amount of moles adsorbed at a given pressure P, q_e (mmol g^{-1}) is maximum adsorption capacity, K_s (bar^{-1}) is the Sips model affinity constant and n is the heterogeneity coefficient where values higher than 1 are attributed to heterogeneous systems, while values close to 1 are associated with homogeneous ones[28]. The parameter n is usually greater than unity, and thus, the higher this parameter, the more heterogeneous the system is [27].

The goodness of fit was evaluated with the residual sum of squares (SSR):

$$SSR(\%) = \left(\frac{\sum_{i=1}^{i=n}(q_{exp\,i} - q_{mod\,i})^2}{N} \right) \cdot 100 \tag{5}$$

where $q_{exp\,i}$ and $q_{mod\,i}$ are the experimental and predicted amounts adsorbed respectively, i represents each pressure considered and N is the total number of experimental data points.

Finally, the corrected Akaike Information Criterion (AICc) [29, 30] and Bayesian Information Criterion (BIC)[31], which are typically used to balance the trade-off between the goodness of fit and simplicity of a particular model, were calculated as follows:

$$AICc = ln\left(\frac{\sum_{i=1}^{i=n}(q_{exp\,i}-q_{mod\,i})^2}{N}\right) + \frac{2\cdot p}{N-p-1} \qquad (6)$$

$$BIC = ln\left(\frac{\sum_{i=1}^{i=n}(q_{exp\,i}-q_{mod\,i})^2}{N}\right) + \frac{2\cdot ln\,(N)}{N} \qquad (7)$$

where $q_{exp\,i}$ and $q_{mod\,i}$ are the experimental and predicted amounts adsorbed respectively, i represents each pressure considered, p is the number of estimated parameters in the model and N is the total number of experimental data points. In this study, the corrected Akaike Information Criterion was calculated due to the sample size (N) is small compared to the number of parameters (N/p < 40).

3. Results and discussion

3.1 Influence of activation conditions on CO_2 uptake.

It is well known that the physicochemical properties of the carbonaceous materials produced will influence their maximum adsorption capacity of CO_2, as previously demonstrated elsewhere [32, 33]. Simultaneously, these properties are clearly dependent on the conditions in which activation takes place; i.e activating agent, activation temperature, holding time, activation agent flow rate and pressure. Thus, to study these influences, experiments were carried out by varying one parameter at a time with the others kept constant for each activating agent. The criterion selected to fix each variable was maximum CO_2 uptake. Then, the samples that displayed highly different adsorption

11

capacities were selected to be further characterised to elucidate their physicochemical properties.

Figure 1 shows CO_2 uptake at different activation temperatures for both activating agents (CO_2 and steam) and Table 3 lists burn-off values for each sample. In this study, three temperatures for H_2O activation (700, 800 and 900 ºC) and five for CO_2 activation (700, 800, 900, 1000 and 1100 ºC) were studied. It can be seen that the activation temperature displayed a significant effect on CO_2 uptake, and was more prominent for CO_2 activation. CO_2 uptake and burn-off values directly increased with temperature, unlike in the activated biochar yield. These results are in close agreement with the literature [5, 6, 34-36].

Regarding CO_2 activation, an increase in temperature from 700 to 1000 ºC, led to a significance rise in CO2 uptake from 1.89 to 4.66 mmol/g and burn-off degree, from 3% to 60% respectively. Meanwhile, the activated biochar yield decreased from 26 to 9.6% for 700 and 1000ºC, respectively. To understand these results, it must be noted that CO_2 activation is based on the Boudouard reaction ($C(s) + CO_2(g) \rightleftharpoons 2CO(g)$), in which the CO_2 reacts with carbon atoms, and this is one of the main mechanisms for micropore development [35]. This reaction is endothermic and this favours the forward reaction at high temperatures, thus causing carbon atoms to be removed and increasing burn-off. However, due to positive enthalpy (+172 kJ/kmol in standard conditions), the equilibrium of this reaction requires temperatures above 700 ºC [37] to produce CO . This observation is coherent with the low burn-off value of the sample activated at 700 ºC (3 %). In addition, CO_2 uptake was only slightly improved in comparison to that obtained without activation (Figures 1 and 5). These findings could indicate that low temperatures were insufficient for developing the porosity desired in the carbon structure (surface area of 18.02 m^2/g) for CO_2 capture. However, the yield of activated biochar at 1100 ºC was

insufficient, which is coherent with the high extent of burn-off, and so it was not possible to measure its physicochemical properties and CO_2 uptake.

As for steam activated materials (Figure 1), the tests showed significant differences between 700 and 900 ºC (2.34 and 3.49 mmol/g for 700 and 900 ºC, respectively) and between 800 and 900 ºC (2.35 mmol/g for 800 ºC). However, similar values were found between 700 and 800 ºC, which could indicate that the porosity of activated biochar tended to increase at very high activation temperatures. However, these yields decreased and burn-off increased. These results can be explained by observing the *Water-Gas* reaction ($C(s) + H_2O\ (g) \rightleftharpoons CO\ (g) + H_2\ (g)$), which is the main one involved in H_2O activation. It is also endothermic (+131 kJ/kmol in standard conditions) and is favoured at high temperatures. Thus, this may indicate that at low temperatures, the steam reacts with disorganised carbons resulting from deposition and tar decomposition, but formation of new pores is negligible [38], while at high temperatures production of new pores is more significant, which means the activated carbon has a well-defined surface (surface area up to 1190 m²/g) [39]. Nonetheless, coherent with some studies reported in the literature [34, 35, 39], excess temperature could destroy micropores, and form meso and macropores. Consequently, the carbon structure could be consumed and, thus, the burn-off value obtained would be close to 100 %, just as what happened with CO_2 activation at 1100 ºC.

Comparing both activating agents, it was seen that CO_2 activation lead to higher CO_2 uptake and higher yields of activated biochar. However, lower burn-off values were obtained, which is in good agreement with the literature [6, 34]. As a result, optimal temperatures were chosen according to the highest CO_2 uptake, and 900 ºC was the temperature selected for steam activation materials while 1000 ºC was selected for CO_2

activation. The lower temperature required for H_2O activation was consistent with the greater reactivity of water vapour in the heterogeneous reaction for steam reforming [6]. Moreover, in these conditions there was an activated biochar yield of 9.6 and 6 wt.% for CO_2 and H_2O activation and a burn-off degree of 60 and 70 %. According to different authors [34, 39], pore size development is related to the degree of burn-off and it can be explained by two simultaneous actions: development and expansion of microporosity. The former predominates in the first stage of activation, hence the low burn-off, while the latter becomes predominant when burn-off ranges from approximately 40-60 %. Thus, values over 60 % could destroy the micropores leading to the formation of mesopores and macropores. Thus, the lower adsorption capacity of H_2O-900-30-0.3-1 could be associated with the formation of mesopores, as shown in the next section.
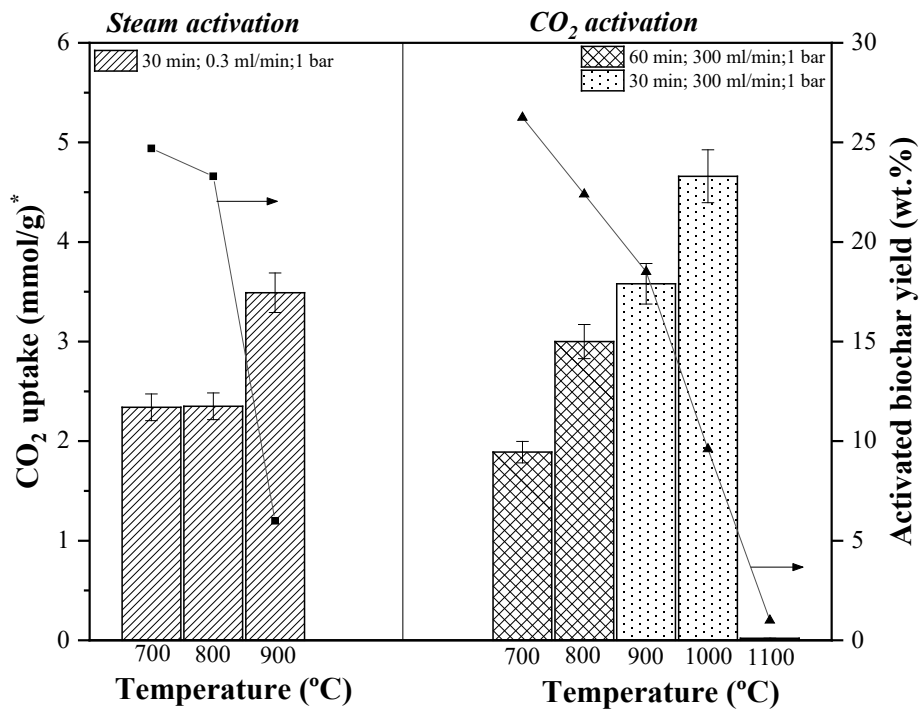
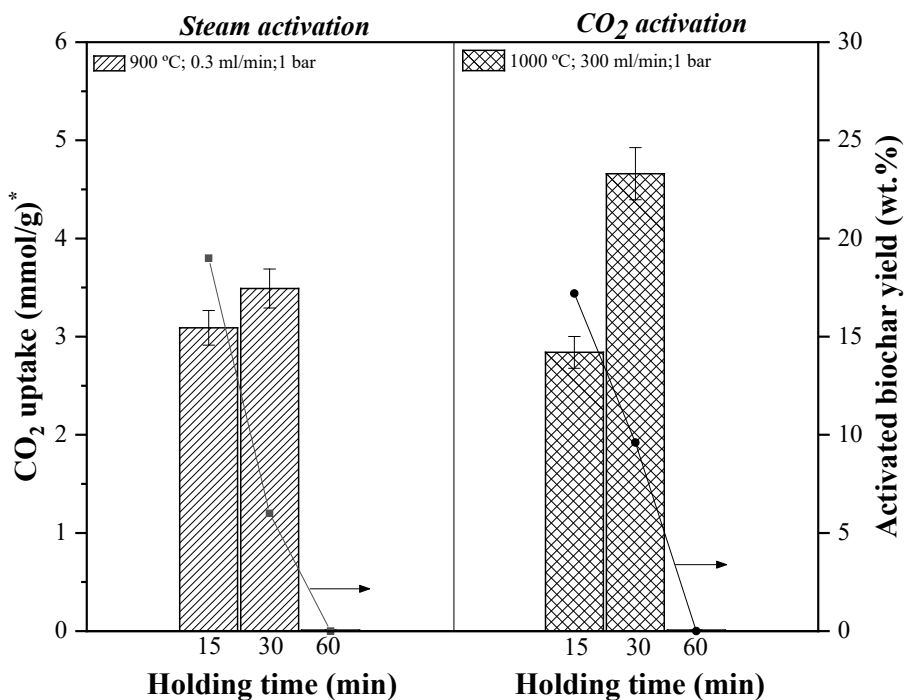*CO_2 adsorption at 30 ºC and 10 bar.

Figure 1. CO_2 uptake at different activating temperatures for steam and CO_2 activation.

Table 3. Burn-off and CO_2 uptake values for activated biochars in different activation conditions.

H₂O activation			
Parameters	***Sample***	***Burn-off (%)***	***CO_2 uptake* (mmol/g)***
Temperature	H_2O-**700**-30-0.3-1	8	2.34
	H_2O-**800**-30-0.3-1	13	2.35
	H_2O-**900**-30-0.3-1	70	3.49
Holding time	H_2O-900-**15**-0.3-1	24	3.09
	H_2O-900-**30**-0.3-1	70	3.49
	H_2O-900-**60**-0.3-1	100	-
H₂O flow rate	H_2O-900-30-**0.07**-1	46	3.61
	H_2O-900-30-**0.15**-1	67	4.28
	H_2O-900-30-**0.3**-1	70	3.49
Pressure	H_2O-900-30-0.15-**1**	67	4.28
	H_2O-900-30-0.15-**10**	17	2.60
CO₂ activation			
Parameters	***Sample***	***Burn-off (%)***	***CO_2 uptake* (mmol/g)***
Temperature	CO_2-**700**-60-300-1	3	1.89
	CO_2-**800**-60-300-1	13	3
	CO_2-**900**-30-300-1	26	3.58
	CO_2-**1000**-30-300-1	60	4.66
	CO_2-**1100**-30-300-1	95	-
Holding time	CO_2-1000-**15**-300-1	32	2.84
	CO_2-1000-**30**-300-1	60	4.66
	CO_2-1000-**60**-300-1	100	-
CO₂ flow rate	CO_2-1000-30-**300**-1	60	4.66
	CO_2-1000-30-**600**-1	68	4.6
	CO_2-1000-30-**900**-1	97	-
Pressure	CO_2-1000-30-300-**1**	60	4.66
	CO_2-1000-30-300-**10**	65	2.53

*CO_2 adsorption at 30 ºC and 10 bar

15

Figure 2 shows the influence of activation holding time for both activating agents. For steam activated materials, the influence of holding time on their CO_2 uptake was less marked than in CO_2 activated materials, and a rise in activation holding time only caused a slight increase in CO_2 uptake. However, greater differences were observed for activated biochar yields and the degree of burn-off. These results can be attributed to activation, since longer holding times leads to a lower yield of activated biochar and, consequently, higher values for burn-off. In addition, at lower times, formation of new pores predominates. However, with long activation times, pore widening becomes the salient feature, whereas pore deepening and new pore formation becomes negligible [35]. In this respect, a holding time of 15 min had low burn-off at 24%, which may indicate formation of the first micropores, but more time was required to develop a good microstructure. Conversely, at 30 min, activated biochar, at 67 %, could be linked to a larger microporous surface, but also to the formation of mesopores, which leads to slightly higher CO_2 uptake. Moreover, at longer times the carbon was totally consumed. In CO_2 activation, a great difference in CO_2 uptake was observed and this could be explained by the extent of burn-off. In sample, CO_2-1000-15-300-1, CO_2 was 32 %, while in sample, CO_2-1000-30-300-1, it was 60 %, which could be due to a more developed microporous surface. Just like for steam, in long reaction times (60 min) the sample became totally gasified and, thus, it could not be evaluated. Finally, due to the higher adsorption capacity, 30 min were selected in both activations.
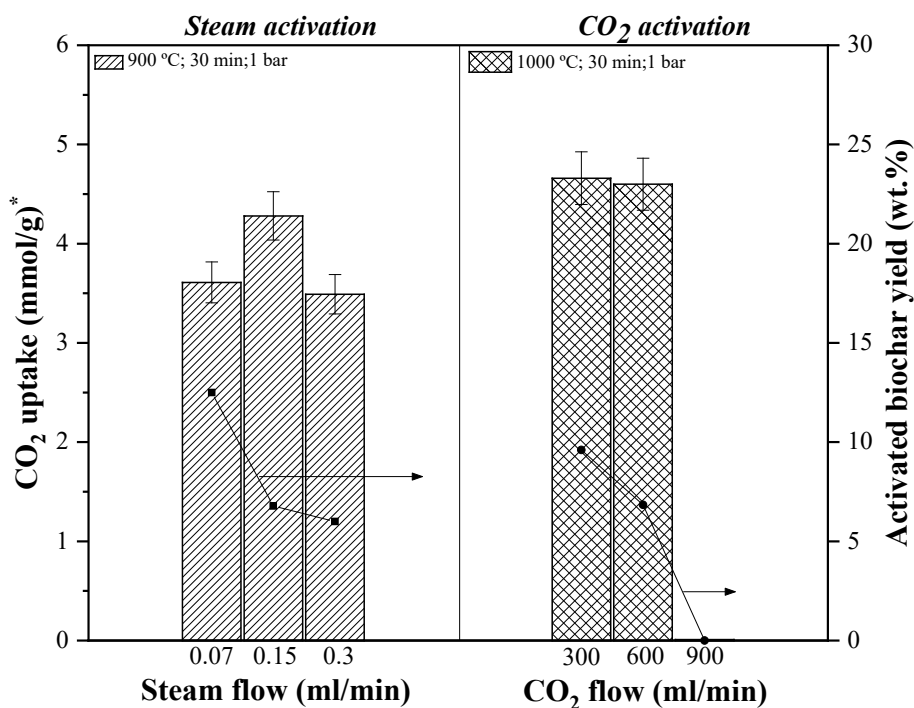
Figure 2. CO_2 uptake at different holding times for steam and CO_2 activation.

Also, the effect of the activating agent flow rate was shown in Figure 3. In the steam flow rate, an increase in CO_2 uptake can be clearly seen, with a maximum value for flow rate at 0.15 ml/min. Additionally, a rise in the steam flow rate caused a higher degree of burn-off, which might be linked to the partial conversion of the micropores into mesopores. In addition, an increase in the amount of steam supplied favours equilibrium in the steam gasification reaction, which can occur so fast, the steam does not have enough time to spread throughout the carbon particle and thus only the outer part is activated [34]. Thus, meso and macropores may develop and, consequently, CO_2 uptake decreases. With the CO_2 activated materials, this uptake was not strongly influenced by flow rate, although yields of activated biochar fell and burn-off rose. This could be associated with the reaction between carbon and CO_2, which could result not only in new micropores, but also to broadening of the existing micropores, which become mesopores, and hence the micropores formed during activation are destroyed. Therefore, based on the results

obtained, flow rates of 0.15 ml/min and 300 ml/min for steam and CO_2 activation, respectively, were selected due to the high CO_2 uptake.
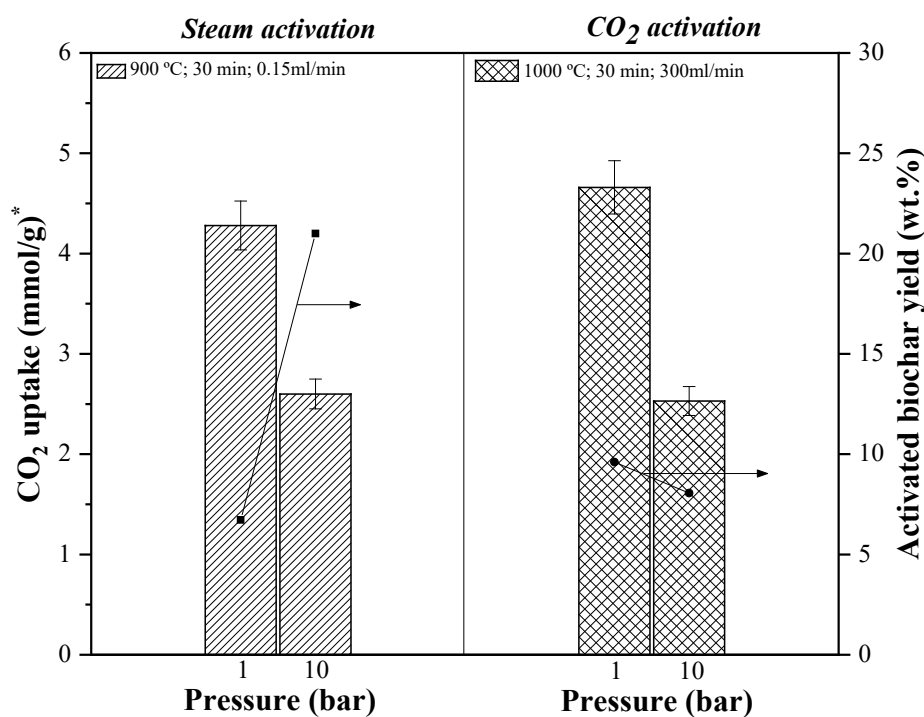

*CO_2 adsorption at 30 ºC and 10 bar.

Figure 3. CO_2 uptake at different steam and CO_2 flow rates.

Finally, Figure 4 shows the results obtained for activation pressure on CO_2 uptake. For CO_2 activated materials, it can be observed that a higher pressure, leads to a lower yield of activated biochar, the degree of burn-off (which indicated that the pressure favoured the Boudouard reaction) and CO_2 uptake. Thus, the effect of partial pressure of CO_2 might have an important influence on the surface chemistry of the materials. In addition, a rise in burn-off ,above 60 % ,at higher pressures could be associated with the formation of mesopores [40] and hence less CO_2 uptake in the end. Otherwise, for H_2O activation, burn-off was considerably lower at higher pressures, which could indicate that the water-gas reaction was favoured at low pressures [41]. Less burn-off at higher pressures (17 %)

could indicate a low degree of micropore formation. As a result, a pressure of 1bar was selected.

*CO_2 adsorption at 30 °C and 10 bar.

Figure 4. CO_2 uptake at different pressures for steam and CO_2 activation.

In short, in this paper the activated carbons H_2O-900-30-0.15-1 (H_2O-AC) and CO_2-1000-30-300-1 (CO_2-AC) were selected as they had the most optimal conditions in terms of their higher CO_2 adsorption capacities. It must be noted that burn-off in this study was in the same range as reported elsewhere [34, 39, 42] for lignocellulosic biomass. Finally, the activated biochar yield was 6 and 9.6 wt.% for H_2O-AC and CO_2-AC, respectively.

To confirm that the activated biochars produced from olive stones and developed in this study could be deemed comparable adsorbents for further higher scale applications, an adsorption experiment with commercial activated carbon under the same conditions (30 °C and 10 bar) was carried out whose results are seen in Figure 5. Additionally, adsorption

capacities of the raw material and the carbonisation material without further activation, were included as blank experiments. It can be observed that biochar activation is needed for successful CO_2 capture. Comparing synthesised activated biochars, it is clear that the CO_2 activated material displayed slightly better adsorption capacity (4.7 mmol/g) than that produced from H_2O activation (4.3 mmol/g) under these experimental conditions. This could be explained by looking at burn-off from the CO_2 activated material, since its value was closer to 60%. Furthermore, the CO_2 adsorption capacity of activated biochars herein have also been compared with biochars prepared by physical activation from other lignocellulosic biomass: vine shoots (3.45 mmol/g at 10 bar and 25 ºC) [43], wood pellets (4mmol/g at 10 bar and 30 ºC)[44] , cherry stones (2.8 mmol/g at 10 bar and 30 ºC)[45], cellulose (3.78 mmol/g at 1 bar and 25 ºC) [46] and coconut Shell (3.9 mmol /g at 1 bar and 25 ºC), [47]. Finally, the adsorption results obtained by the commercial activated carbon (4.9 mmol/g) showed that the activated biochars produced in this study could be considered as potential materials for further industrial applications, since they mostly display the same adsorption capacity.
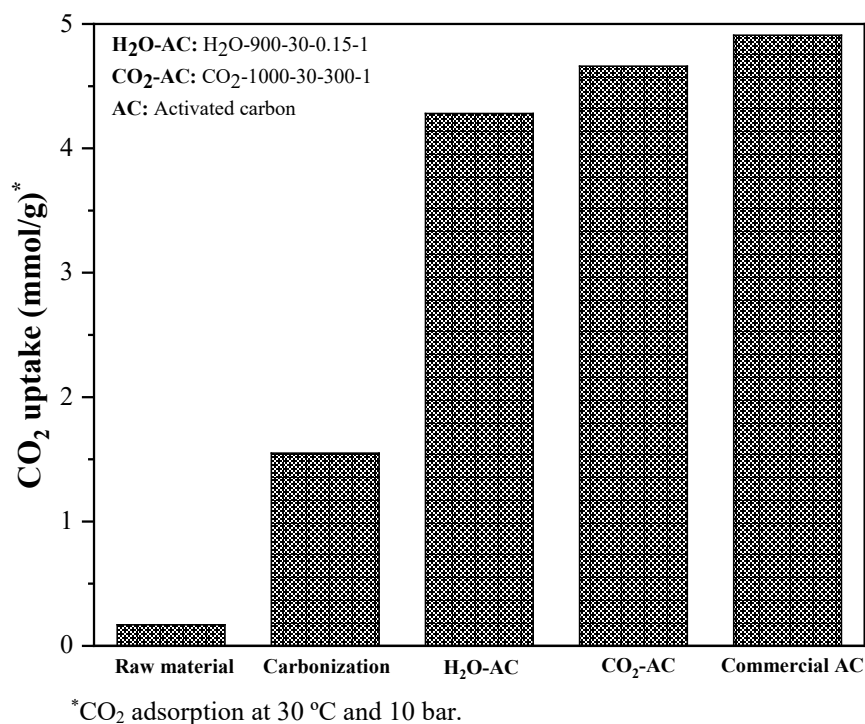
Figure 5. CO_2 uptake for raw material, carbonisation, activated biochars selected and commercial activated carbon.

3.2 Characterisation of selected biochar materials

Figure 6 and Table 4 show the textural properties of the selected carbonaceous materials. Regarding biochar materials activated by steam flow (Figure 6 (a) and Table 4), they clearly show an adsorption isotherm Type I, which is characteristic of high microporous materials. This high N_2 adsorption at a very low P/P_0 ratio is distinctive of materials with narrow micropores with a width of ~1 nm [48]. This pore diameter value (dp) is coherent with the results obtained and shown in Table 4 (1.20-1.87 nm). For materials produced at higher temperatures (900 °C) and at lower pressures (1 bar), H_2O-900-30-0.15-1 and H_2O-900-30-0.3-1, larger H4 hysteres loops were detected, which are characteristic of microporous materials with some mesoporosity, based on the IUPAC classification [48]. These materials have a greater volume of mesopores in comparison to the other samples, 0.17 cm^3/g and 0.12 cm^3/g, respectively. Additionally, these biochar materials, are greater

21

in terms of pore volume (0.69 and 0.60 cm^3/g), external surface area (632 and 546 m^2/g) and specific surface area values (1190 and 1125 m^2/g) in comparison to the other steam flow activated biochars. Regarding the biochar produced at 10 bar, H_2O-900-30-0.15-10, an important decrease in its volume of mesopores (0.05 cm^3/g), specific surface area (695.12 m^2/g) and pore volume (0.33 cm^3/g) can be seen in H_2O-900-30-0.15-1. CO_2 activated biochar materials shown microporous structures described by Type I isotherms without a hysteresis loop. As with steam flow activated biochars, N_2 adsorption at very low P/P_0 describes narrow micropores with a width of ~1 nm, (1.03-1.58 nm) [48]. Here, the widest pore diameter was found with the biochar produced at 10 bar, CO_2-1000-30-300-10. In general, these materials do not have significant mesoporosity ($\leq$ 0.4 cm^3/g) even at higher temperatures, since most of the pore volume is microporous (> 87%), which provides a more uniform structure in comparison to steam activated materials. The specific surface area values of these biochar materials are lower than those obtained by steam activation. Additionally, the rise in temperature from 700 to 900 and 1000 °C during activation shows a highly positive effect on the texture properties of the resulting materials, and specific surface area values of 944.30 and 955.06 m^2/g, respectively were reached.
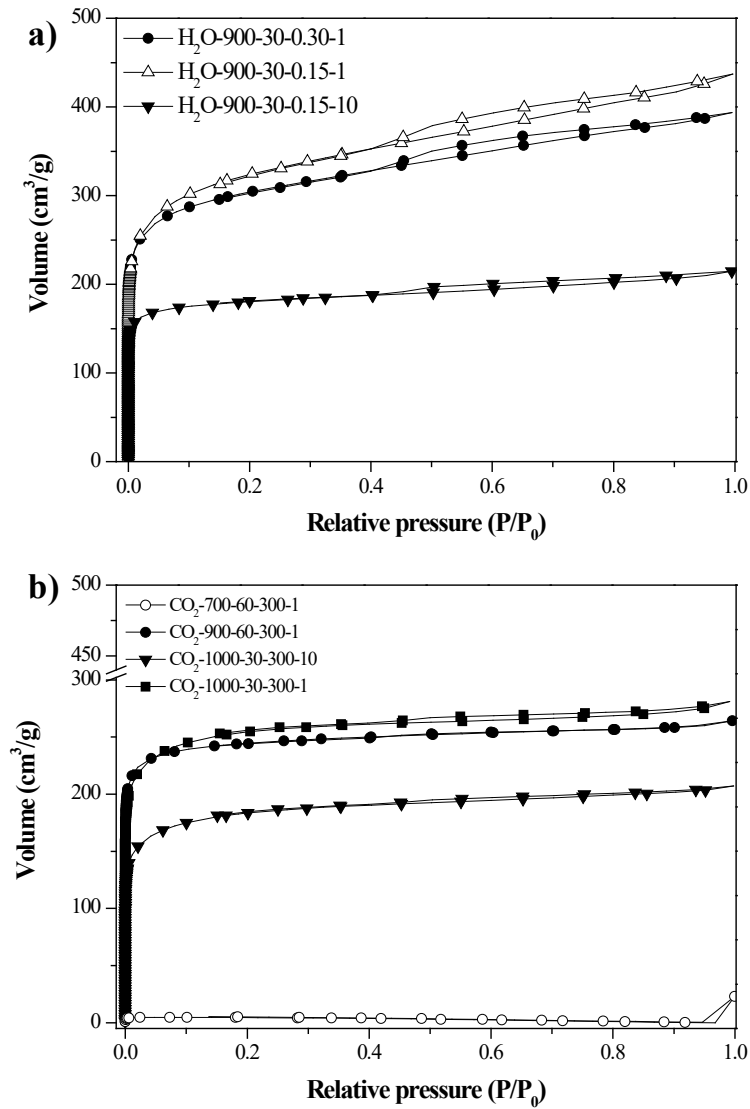
Figure 6. Adsorption-desorption isotherms for N_2 at -196 °C for biochar materials activated by H_2O steam (a) and CO_2 flow (b).

As with steam activated materials, at higher pressures, there is a sharp fall in the volume of pores and the specific and external surface area values for the biochar, so this increase in operational pressure does not enhance the texture properties in the material. Thus, the biochar activated by an CO_2 flow of 300 ml/min at 1000 °C and 1 bar for 30 min, shows texture properties with great potential for CO_2 capture at 10 bar and 30 °C, which is in keeping with the results reported in Section 3.1.

Table 4. Texture properties of the biochars produced by H_2O and CO_2 activation.

	Sample	S_{BET} (m²/g)	dp (nm)	S_{mic} (m²/g)	S_{ext} (m²/g)	V_{pore} (cm³/g)	V_{micro} (cm³/g)	V_{meso} (cm³/g)
	Carbonization	6.40	-	-	-	-	-	
H_2O activation	H_2O-900-30-0.3-1	1125.05	1.68	579.04	546.01	0.60	0.48	0.12
	H_2O-900-30-0.15-1	1190.65	1.87	558.47	632.18	0.69	0.52	0.17
	H_2O-900-30-0.15-10	695.12	1.20	467.30	227.82	0.33	0.28	0.05
CO_2 activation	CO_2-700-60-300-1	18.02	-	-	-	-	-	
	CO_2-900-60-300-1	944.30	1.03	696.05	248.25	0.41	0.38	0.03
	CO_2-1000-30-300-1	955.06	1.46	552.45	402.61	0.44	0.40	0.04
	CO_2-1000-30-300-10	685.03	1.58	370.06	314.97	0.32	0.28	0.04

Figure 7 shows HRSEM micrographs of the most representative selected materials: olive stone, carbonisation, H_2O-900-30-0.15-1, H_2O-900-30-0.15-10, CO_2-700-60-300-1 and CO_2-1000-30-300-1 (Figure 7). After carbonising the olive stone, the porosity of the biochar was not developed, which is consistent with our previous results on texture (Table 4). However, highly porous structures were obtained when physical activation, both CO_2 and H_2O, was used. This highly porous structure was not produced for CO_2-1000-30-300-10 and H_2O-900-30-0.15-10, so a rise in pressure during the process reduced biochar porosity. These results are also coherent with our previous outcomes for textures.
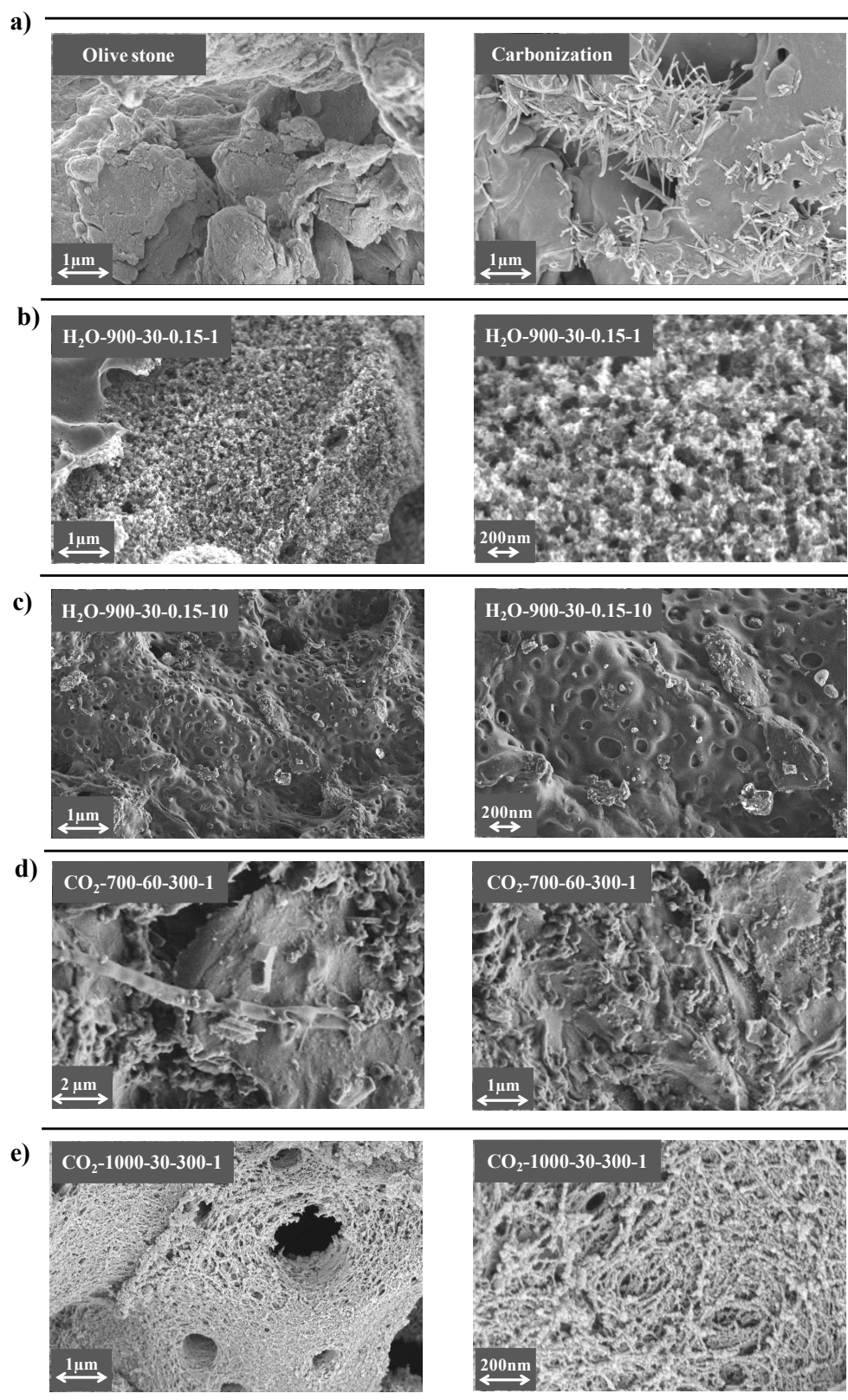
Figure 7. HRSEM micrographs of Olive stone (a left), Carbonisation (a right), H_2O-900-30-0.15-1 (b), H_2O-900-30-0.15-10 (c), CO_2-700-60-300-1 (d) and CO_2-1000-30-300-1 (e).

Moreover, as for the CO_2 activated biochar, temperature significantly affected their texture properties. Therefore, CO_2-700-60-300-1 and CO_2-1000-30-300-1 were selected. It is evident that CO_2 activation at 700 °C was not linked to more porosity in the material (Figure 7 d). However, micrographs of the material activated at 1000 °C perfectly describes the results obtained from the experiments on texture, thereby revealing a highly uniform structure, small pore size and high volume of pores (Figure 7 e).

Raman spectra of biochar materials selected are shown in Figure 8. The carbonisation spectrum was also added for comparison purposes. In all cases, two main bands were detected. As explained by Umesh Agarwal [49], the band located at ~1600/1595 cm^{-1} is characteristic of the stretching mode of sp^2 aromatic rings in lignin. Otherwise, the band centred at ~1334 cm^{-1} can mainly be attributed to the bending mode of aliphatic O-H groups. Additionally, the shoulder found at ~ 1195 cm^{-1} can be assigned to the phenolic groups contained in these lignin-based materials. Therefore, as with carbon-based materials, the ratio between the intensities of more disordered (O-functional groups) band (D) and the sp^2 aromatic and more ordered band (G) shows the amount of defects (I_D/I_G)[50]. It can be seen that I_D/I_G values obtained from activated biochars are greater in comparison to that material which has only undergone carbonisation (Figure 8). Biochars activated by both gases show that an increase in temperature led to a rise in the amount of defects in the material. This may be related to greater porosity in the material, as shown in Table 4 and Figure 7.
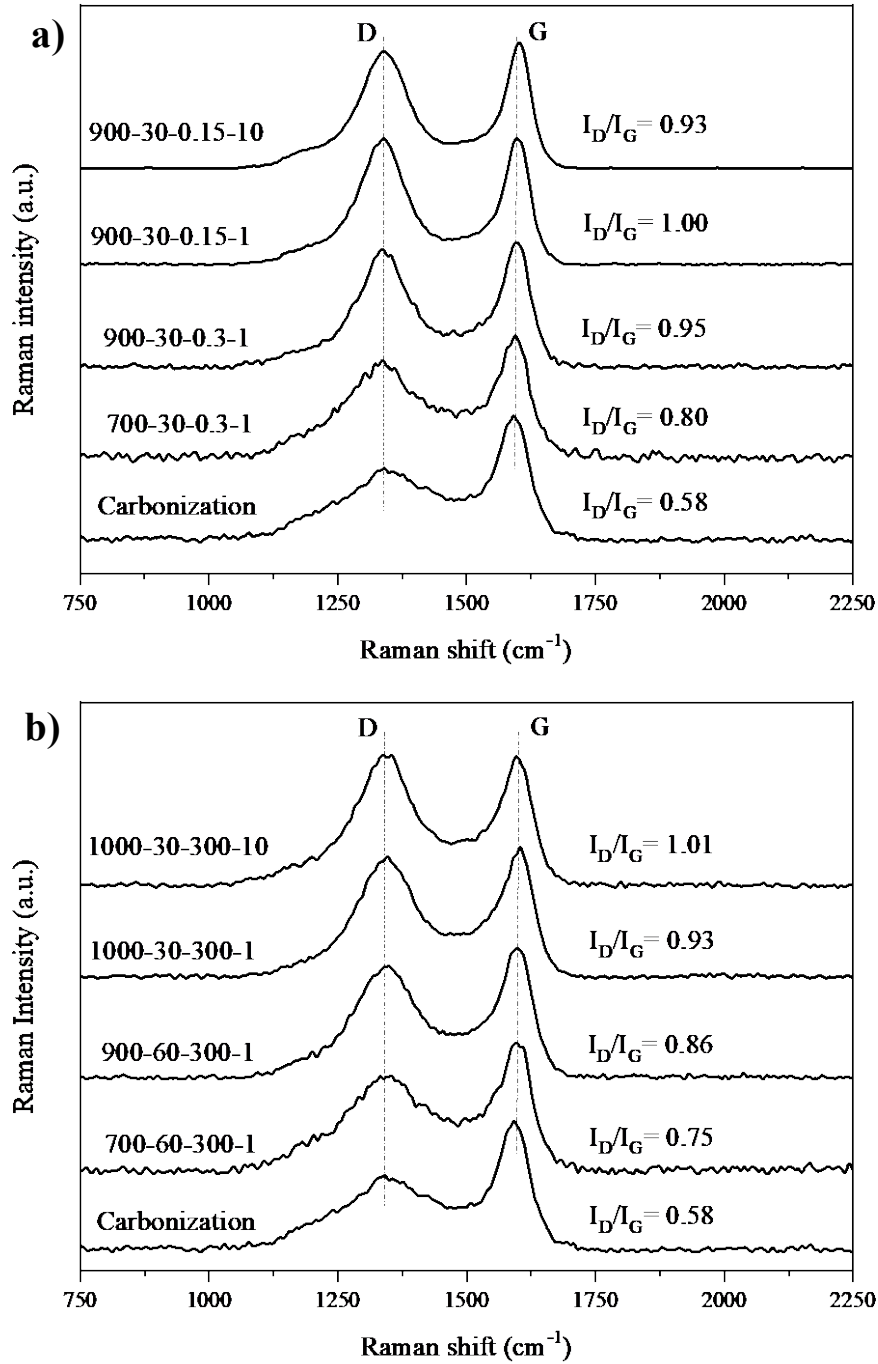
Figure 8. Raman spectra of biochar materials activated by H_2O steam (a) and CO_2 (b)

flow.

As for the biochars produced at different pressures (1-10 bar), it has been shown that

varying results are obtained depending on the activating gas selected. For steam activated

biochar, there is a decrease in the I_D/I_G value (0.93) in comparison to the result obtained

by CO_2 activated material (1.01), so more materials with defects were found to have a wider pore diameter (Table 4).

Thermal stability tests for these biochars are presented in Figure 9 and Figure 9 a) shows that the olive stone starts combustion earlier than with carbonised biochar. After carbonisation most of its oxygen functionalities were removed and consequently, a more stable material was obtained. The DTG of the olive stone went through four main stages of decomposition. The first occurred at ~120 ºC, which was related to drying. The second covered temperatures between 220-400 ºC, which corresponded with removing volatile matter, leading to char formation. At this stage, the decomposition of hemicellulose took place at temperature between 220-315 °C, whereas cellulose decomposition occurred at 315-400 ºC. Next, lignin (stage three) decomposition took place between 220-770 °C [51-54]. At the last stage, between 400-500 ºC, the char was ignited after the volatile matter was removed.

Previously, a rise in activation temperature using both steam and CO_2 was seen to develop better texture (Table 4) and structural (Figure 8) properties in the biochar. Raman spectroscopy showed that materials with most defects were found after this increase. This finding was directly correlated to an increase in the pore width of the material.
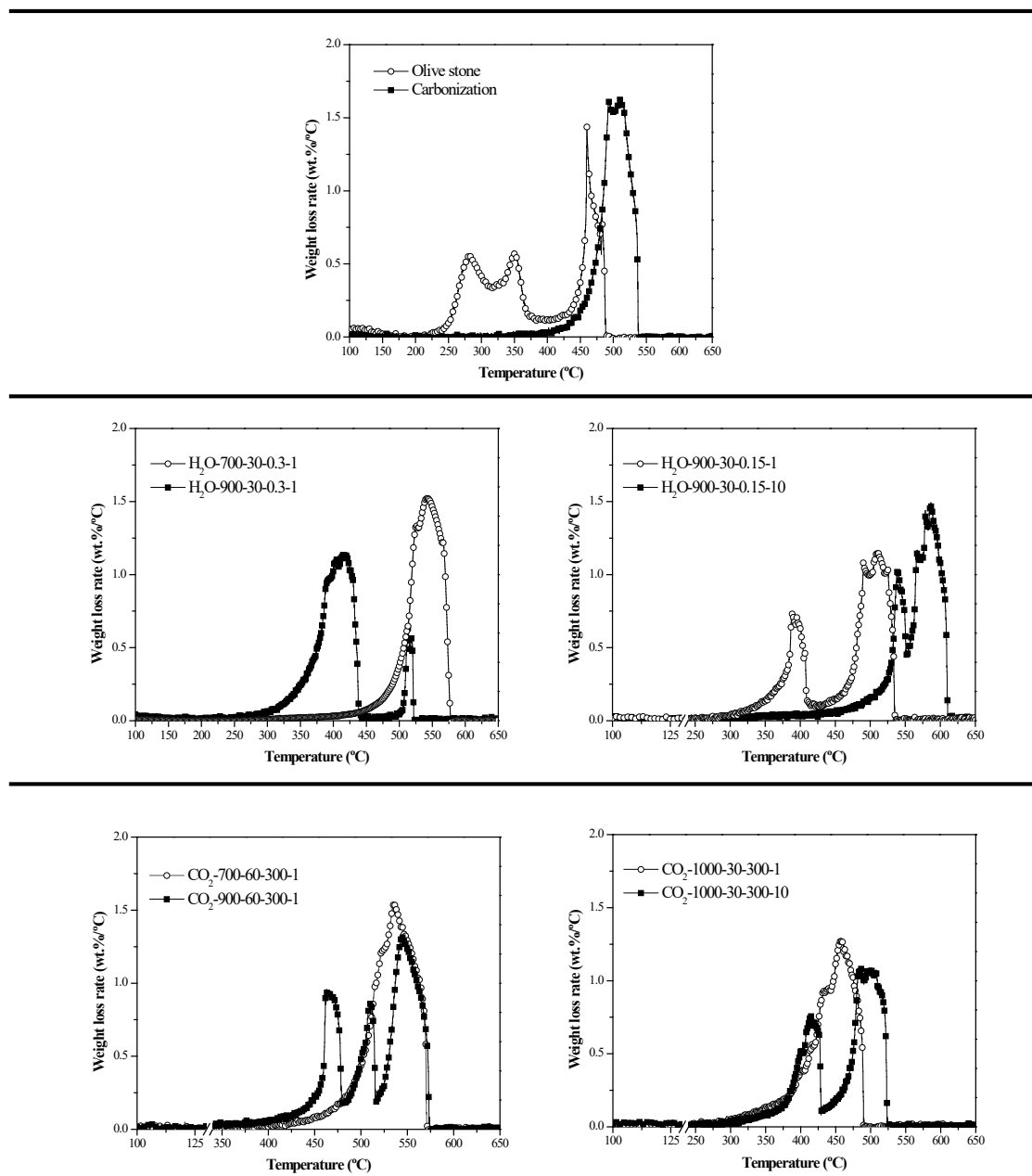
Figure 9. Derivative thermogravimetric (DTG) curves for: a) raw material and carbonisation; b) H_2O activation; c) CO_2 activation.

On the left side of Figure 9 a) and Figure 9 b) the effect of activation temperature with steam and CO_2, respectively, on the thermal stability of these biochars, is shown. In both cases, materials with higher amounts of defects and bigger pore widths burn faster. According to research by Gani and Naruse , an increase in the pore width of the biochar would help oxygen to be diffused throughout the pores, thereby enabling the lignin

components of the biochar to react more easily [55]. As seen in the right column of Figure 9 a) and Figure 9 b), this hypothesis is also consistent with the DTG results obtained for biochars activated at different pressures (1-10 bar).

The Van Krevelen diagram (H/C vs O/C) for the selected biochars is shown in Figure 10. Note that after carbonisation at 600 ºC, there is a sharp drop in H/C and O/C from the olive stone (Table 1), which are coherent with previous results published elsewhere [56]. Different values for these are obtained depending on the type of gas used - steam or CO_2 - for activating the biochar. Results are shown in Figure 10 a) and Figure 10 b), respectively. In any event, the H/C value falls after a rise in activation temperature. Additionally, greater O/C values are obtained for biochars activated at 900 ºC (0.044) in comparison to 700 ºC (0.018). Rodriguez-Reinoso et al. concluded that the inhibition effect of hydrogen produced in the water-gas shift reaction during steam activation, is minimised at high temperatures [57]. Therefore, this enhances the oxidation reaction on the carbonaceous surface, thereby producing greater values for O/C. These outcomes concur with those obtained by Raman (Figure 8) and DTG (Figure 9) experiments, since both materials have the highest amount of defects and quickest burn-off temperature for steam activated biochars. Otherwise, this O/C value falls to 0.019 for H_2O-900-30-0.15-10 due to the dehydration reaction that occurs on the surface of the material.

Moreover, an increase in activation temperature from 700 to 900 ºC leads to lower H/C and O/C values for CO_2 activated biochars. This finding can be explained in light of the Boudouard reaction, since CO production is favoured at temperatures above 700 ºC [37], leading to greater burn-off. Additionally, this reaction seems to be favoured at higher activation pressures, since CO_2-1000-30-300-10 shows the highest O/C value due to greater oxidation in the material. This result is also consistent with that obtained by

Raman and the DTG analysis, since this material shows the highest I_D/I_G value and quickest burn-off temperature.
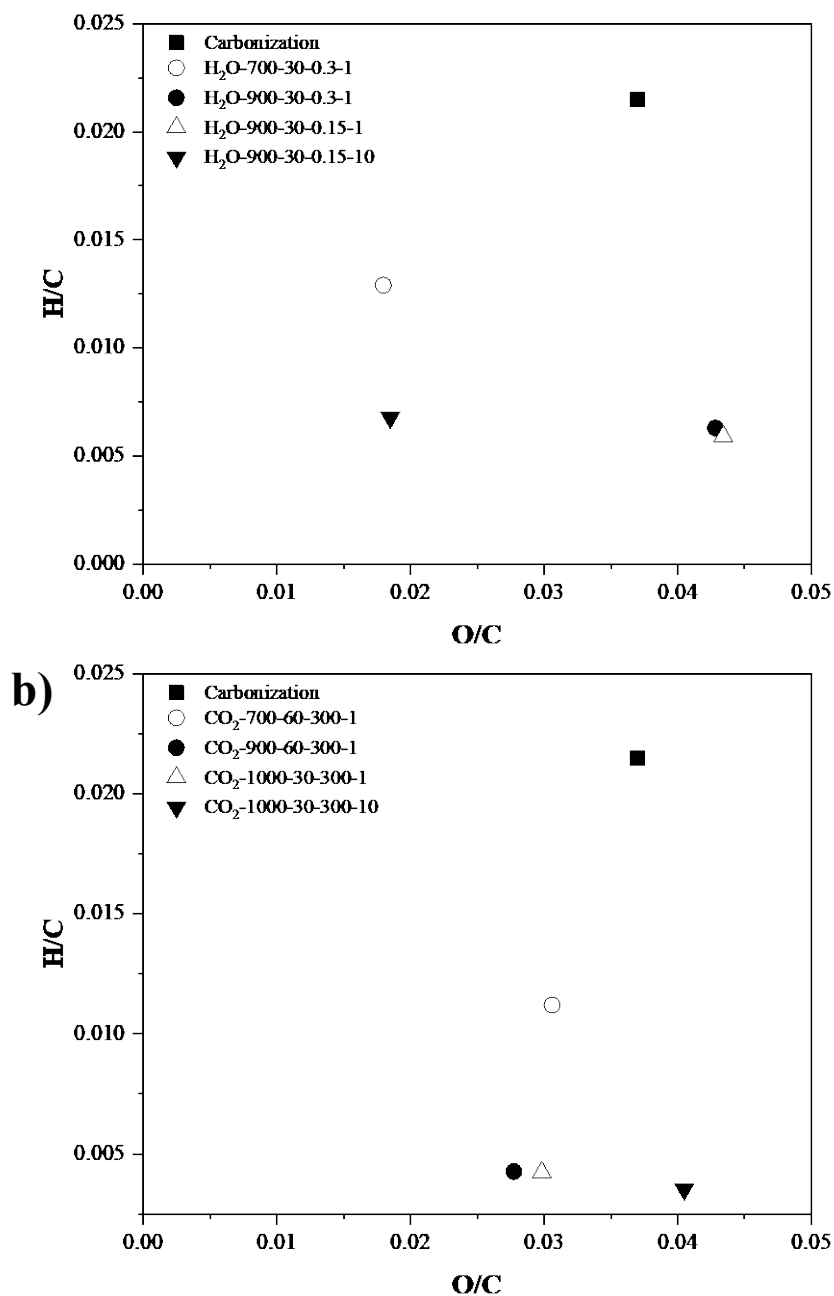

Figure 10. Van Krevelen diagram: a) H_2O activation and b) CO_2 activation

3.3 Equilibrium of CO_2 adsorption

The CO_2 adsorption isotherms over the pressure range of 1-20 bar at 30 ºC for samples H2O-900-30-0.15-1 and CO2-1000-30-300-1 are shown in Figure 11. For both biochars, higher CO_2 uptake were found, as the pressure in the system increased which is because adsorption is exothermic [58]. Nonetheless, the slope of the isotherm decreased at higher pressures since adsorption sites were then approaching saturation. In addition, note that maximum adsorption capacity was reached around 10 bar, since there was no improvement in the adsorbed amount at higher pressures. Moreover, the adsorption isotherms also showed that under the same conditions, the amount of CO_2 uptake was slightly higher for the biochar obtained by CO_2 activation, which is coherent with differences found in the total volume of micropores (75 % for H_2O activated material and 91% for CO_2 activated material) and similar conclusions were obtained elsewhere [59]. The predicted amounts adsorbed from Langmuir, Freundlich and Sips models and the estimated fitting parameters are also plotted in Figure 11. SSR values are summarized in Table 5.
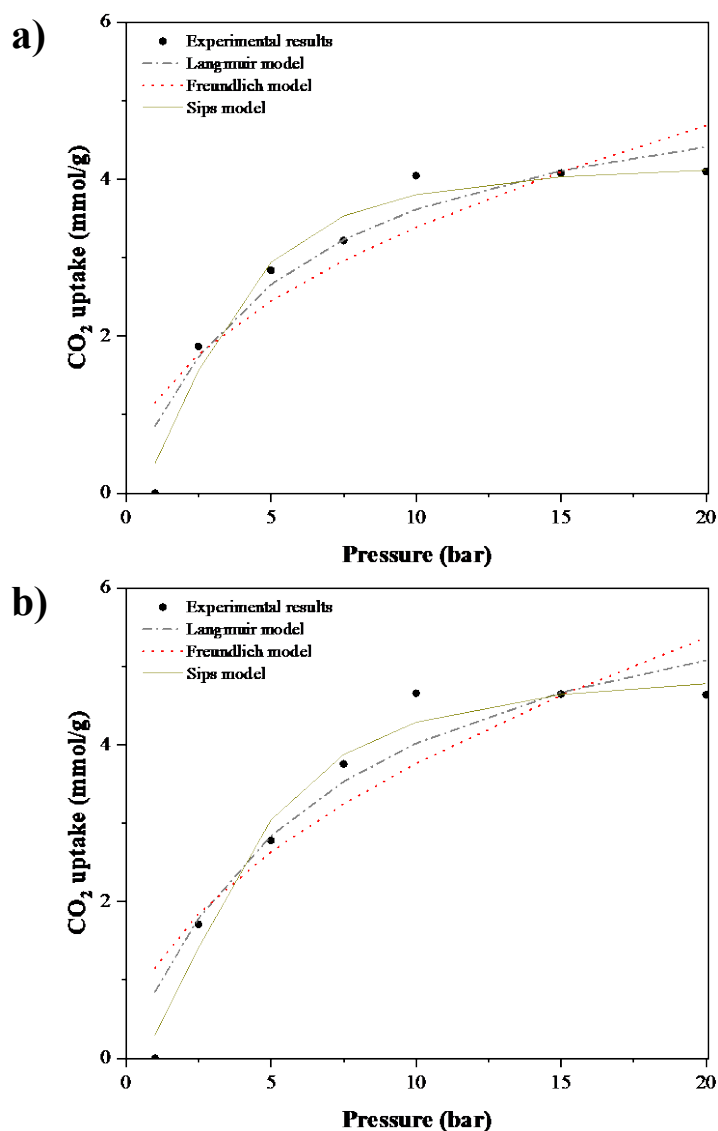
Figure 11. Adsorption equilibrium isotherms for CO_2: a) H_2O-900-30-0.15-1 and b) CO_2-1000-30-300-1.

As seen in Figure 11, the Freundlich and Langmuir models were not a good model for CO_2 adsorption for these activated biochars, while the Sips model perfectly fitted the experimental data, demonstrating that the latter could be employed to accurately correlate the adsorption equilibria. In addition, goodness of fit is corroborated by the low values obtained for the SSR, AICc and BIC (Table 5) in comparison to the other models.

Moreover, on comparing the main parameters of the Sips model for both adsorbents (Table 5) the maximum amount of sample CO_2-1000-30-300-1 adsorbed was found to be

higher than in H_2O-900-30-0.15-1, while parameter n from the Sips model, which reflects system heterogeneity, were practically equal between both activated biochar. This finding suggested that heterogeneity and interaction between CO_2 and biochars were similar for both adsorbents. Finally, the affinity parameter (K_S) was higher for CO_2-1000-30-300-1 which can be ascribed to the higher coverage and the greater affinity of the adsorbate to the adsorbent surface.

Table 5. Fitting parameters of Langmuir, Freundlich and Sips models to CO_2 adsorption for biochars H_2O-900-30-0.15-1 and CO_2-1000-30-300-1.

Sample	Model	q_e (mmol/g)	b/Ks (bar^{-1})	K_F (mmol·g^{-1}·bar$^{-1/n}$)	n	SSR (%)	Deviation	AICc	BIC
H_2O-900-30-0.15-1	Langmuir	5.65	0.18	-	-	15	0.29	-0.62	-1.07
	Freundlich	-	-	1.15	2.14	33	0.19	0.14	-0.30
	Sips	4.24	0.30	-	0.51	6	0.12	-0.82	-1.98
CO_2-1000-30-300-1	Langmuir	6.89	0.14	-	-	20	0.22	-0.10	-0.53
	Freundlich	-	-	1.15	1.95	42	0.33	-0.86	-1.33
	Sips	4.98	0.25	-	0.52	6	0.12	-0.85	-2.01

4. Conclusions

In this paper, the effect activation conditions for activated biochar derived from olive stone had on CO_2 uptake, burn-off degree and physicochemical properties was evaluated. It can be concluded that all variables showed a remarkable effect on the morphology and adsorption capacity of activated biochar. In this respect, the activation conditions that maximised CO2 adsorption capacity at 30 ºC and 10 bar were 900 ºC, 30 min, 0.15 ml/min and 1 bar (H_2O-AC) for H20 activation and 1000 ºC, 30 min, 300 ml/min and 1 bar (CO_2-AC)for C02 activation. Moreover, these activated biochars showed a CO_2 adsorption capacity of 4.28 and 4.66 mmol/g, activated biochar yields of 9.6 and 6 wt.% and a burn-off degree of 60 and 67 % for CO_2 and steam activation, respectively. Results for texture revealed that CO_2 activation only favoured development of microporosity, whereas both micropores and mesopores were detected after steam activation. Furthermore, the CO_2 activated carbon was more uniform in structure, with smaller pore size, a higher volume of pores and less defects than in H_2O-AC. In addition, the CO_2 adsorption isotherms in the pressure range of 1-20 bar at 30 ºC demonstrated that both activated biochars reached maximum adsorption capacity at 10 bar. Finally, these adsorption isotherms results were a better fit for the Sips model, with the CO_2-AC sample showing the maximum adsorption capacity and the highest affinity parameter value. In summary, a priori, olive stone may be considered a good precursor for producing low-cost biochar adsorbents, especially when CO_2 is used as the activating agent which reached adsorption capacities that were very similar to those of commercial activated carbons (4.7 and 4.9 for activated biochar from olive pomace and commercial activated carbon, respectively).

References

[1] N. Álvarez-Gutiérrez, M.V. Gil, F. Rubiera, C. Pevida. Kinetics of CO2 adsorption on cherry stone-based carbons in CO2/CH4 separations. Chemical Engineering Journal. 307 (2017) 249-57.

[2] P. Lahijani, M. Mohammadi, A.R. Mohamed. Metal incorporated biochar as a potential adsorbent for high capacity CO2 capture at ambient condition. Journal of CO2 Utilization. 26 (2018) 281-93.

[3] J. Saleem, U.B. Shahid, M. Hijab, H. Mackey, G. McKay. Production and applications of activated carbons as adsorbents from olive stones. Biomass Conversion and Biorefinery. 9 (2019) 775-802.

[4] A. Esteban-Arranz, D. Compte-Tordesillas, V. Muñoz-Andrés, M. Pérez-Cadenas, A. Guerrero-Ruiz. Effect of surface, structural and textural properties of graphenic materials over cooperative and synergetic adsorptions of two chloroaromatic compounds from aqueous solution. Catalysis Today. 301 (2018) 104-11.

[5] M.G. Plaza, I. Durán, F. Rubiera, C. Pevida. CO2 adsorbent pellets produced from pine sawdust: Effect of coal tar pitch addition. Applied Energy. 144 (2015) 182-92.

[6] J. Pallarés, A. González-Cencerrado, I. Arauzo. Production and characterization of activated carbon from barley straw by physical activation with carbon dioxide and steam. Biomass and Bioenergy. 115 (2018) 64-73.

[7] A. Aydin, Y. Bulut, O. Yavuz. Acid dyes removal using low cost adsorbents. International journal of environment and pollution. 21 (2004) 97-104.

[8] O. Ioannidou, A. Zabaniotou. Agricultural residues as precursors for activated carbon production—A review. Renewable and Sustainable Energy Reviews. 11 (2007) 1966-2005.

[9] C. Namasivayam, N. Muniasamy, K. Gayatri, M. Rani, K. Ranganathan. Removal of dyes from aqueous solutions by cellulosic waste orange peel. Bioresource Technology. 57 (1996) 37-43.

[10] N. Álvarez-Gutiérrez, M. Victoria Gil, F. Rubiera, C. Pevida. Cherry-stones-based activated carbons as potential adsorbents for CO2/CH4 separation: effect of the activation parameters. Greenhouse Gases: Science and Technology. 5 (2015) 812-25.

[11] A.E. Ogungbenro, D.V. Quang, K. Al-Ali, M.R.M. Abu-Zahra. Activated Carbon from Date Seeds for CO2 Capture Applications. Energy Procedia. 114 (2017) 2313-21.

[12] E. Menya, P.W. Olupot, H. Storz, M. Lubwama, Y. Kiros. Characterization and alkaline pretreatment of rice husk varieties in Uganda for potential utilization as precursors in the production of activated carbon and other value-added products. Waste Management. 81 (2018) 104-16.

[13] M.M. Alam, M.A. Hossain, M.D. Hossain, M.A.H. Johir, J. Hossen, M.S. Rahman, et al. The Potentiality of Rice Husk-Derived Activated Carbon: From Synthesis to Application. Processes. 8 (2020) 203.

[14] D. Kalderis, D. Koutoulakis, P. Paraskeva, E. Diamadopoulos, E. Otal, J.O.d. Valle, et al. Adsorption of polluting substances on activated carbons prepared from rice husk and sugarcane bagasse. Chemical Engineering Journal. 144 (2008) 42-50.

[15] E. Commission. Short-term outlook for EU agricultural markets. https://ec.europa.eu/info/food-farming-fisheries/farming/facts-and-figures/markets/outlook/short-term_en2019.

[16] G.R. Surup, H.K. Nielsen, M. Heidelmann, A. Trubetskaya. Characterization and reactivity of charcoal from high temperature pyrolysis (800–1600° C). Fuel. 235 (2019) 1544-54.

[17] Y. Kim, J.-I. Oh, M. Vithanage, Y.-K. Park, J. Lee, E.E. Kwon. Modification of biochar properties using CO_2. Chemical Engineering Journal. 372 (2019) 383-9.

[18] Y. You, X. Zhang, P. Li, F. Lei, J. Jiang. Co-production of xylooligosaccharides and activated carbons from Camellia oleifera shell treated by the catalysis and activation of zinc chloride. Bioresource Technology. (2020) 123131.

[19] E. Santos-Clotas, A. Cabrera-Codony, B. Ruiz, E. Fuente, M.J. Martín. Sewage biogas efficient purification by means of lignocellulosic waste-based activated carbons. Bioresource Technology. 275 (2019) 207-15.

[20] D. Peredo-Mancilla, I. Ghouma, C. Hort, C.M. Ghimbeu, M. Jeguirim, D. Bessieres. CO_2 and CH_4 Adsorption Behavior of Biomass-Based Activated Carbons. Energies. 11 (2018) 3136.

[21] M.G. Plaza, F. Rubiera. Evaluation of a novel multibed heat-integrated vacuum and temperature swing adsorption post-combustion CO_2 capture process. Applied Energy. 250 (2019) 916-25.

[22] K. Yang, J. Peng, H. Xia, L. Zhang, C. Srinivasakannan, S. Guo. Textural characteristics of activated carbon by single step CO_2 activation from coconut shells. Journal of the Taiwan Institute of Chemical Engineers. 41 (2010) 367-72.

[23] M. Puig-Gamero, M. Fernandez-Lopez, P. Sánchez, J.L. Valverde, L. Sanchez-Silva. Pyrolysis process using a bench scale high pressure thermobalance. Fuel Processing Technology. 167 (2017) 345-54.

[24] I. Langmuir. The constitution and fundamental properties of solids and liquids. Part I. Solids. Journal of the American chemical society. 38 (1916) 2221-95.

[25] H. Freundlich. Over the adsorption in solution. J Phys Chem. 57 (1906) 1100-7.

[26] S. Chowdhury, R. Mishra, P. Saha, P. Kushwaha. Adsorption thermodynamics, kinetics and isosteric heat of adsorption of malachite green onto chemically modified rice husk. Desalination. 265 (2011) 159-68.

[27] R. Sips. On the structure of a catalyst surface. The Journal of Chemical Physics. 16 (1948) 490-5.

[28] W. Rudzinski, D. Everett. The Empirical Adsorption Isotherms. Adsorption of Gases on Heterogeneous Surfaces, WRH EVERETT, ed(London: Academic Press). (1992) 35-58.

[29] N. Sugiura. Further analysts of the data by akaike's information criterion and the finite corrections: Further analysts of the data by akaike's. Communications in Statistics-Theory and Methods. 7 (1978) 13-26.

[30] H. Akaike. A new look at the statistical model identification. IEEE transactions on automatic control. 19 (1974) 716-23.

[31] G. Schwarz. Estimating the dimension of a model. The annals of statistics. 6 (1978) 461-4.

[32] A.D. Igalavithana, S.W. Choi, J. Shang, A. Hanif, P.D. Dissanayake, D.C.W. Tsang, et al. Carbon dioxide capture in biochar produced from pine sawdust and paper mill sludge: Effect of porous structure and surface chemistry. Science of The Total Environment. 739 (2020) 139845.

[33] P.D. Dissanayake, S.W. Choi, A.D. Igalavithana, X. Yang, D.C.W. Tsang, C.-H. Wang, et al. Sustainable gasification biochar as a high efficiency adsorbent for CO2 capture: A facile method to designer biochar fabrication. Renewable and Sustainable Energy Reviews. 124 (2020) 109785.

[34] S. Román, J.F. González, C.M. González-García, F. Zamora. Control of pore development during CO2 and steam activation of olive stones. Fuel Processing Technology. 89 (2008) 715-20.

[35] F.L. Braghiroli, H. Bouafif, N. Hamza, B. Bouslimi, C.M. Neculita, A. Koubaa. The influence of pilot-scale pyro-gasification and activation conditions on porosity development in activated biochars. Biomass and Bioenergy. 118 (2018) 105-14.

[36] C.-F. Chang, C.-Y. Chang, W.-T. Tsai. Effects of burn-off and activation temperature on preparation of activated carbon from corn cob agrowaste by CO2 and steam. Journal of colloid and interface science. 232 (2000) 45-9.

[37] J. Hunt, A. Ferrari, A. Lita, M. Crosswhite, B. Ashley, A. Stiegman. Microwave-specific enhancement of the carbon–carbon dioxide (Boudouard) reaction. The Journal of Physical Chemistry C. 117 (2013) 26871-80.

[38] B.t. Cagnon, X. Py, A. Guillot, F. Stoeckli. The effect of the carbonization/activation procedure on the microporous texture of the subsequent chars and active carbons. Microporous and Mesoporous Materials. 57 (2003) 273-82.

[39] Y.-J. Zhang, Z.-J. Xing, Z.-K. Duan, L. Meng, Y. Wang. Effects of steam activation on the pore structure and surface chemistry of activated carbon derived from bamboo waste. Applied Surface Science. 315 (2014) 279-86.

[40] S.M. Gouws, H.W. Neomagus, D.G. Roberts, J.R. Bunt, R.C. Everson. The effect of carbon dioxide partial pressure on the gasification rate and pore development of Highveld coal chars at elevated pressures. Fuel Processing Technology. 179 (2018) 1-9.

[41] R. Zagorščak, S. Sadasivam, H.R. Thomas, K. Stańczyk, K. Kapusta. Experimental study of underground coal gasification (UCG) of a high-rank coal using atmospheric and high-pressure conditions in an ex-situ reactor. Fuel. 270 (2020) 117490.

[42] J.E. Vargas, L.G. Gutierrez, J.C. Moreno-Piraján. Preparation of activated carbons from seeds of Mucuna mutisiana by physical activation with steam. Journal of Analytical and Applied Pyrolysis. 89 (2010) 307-12.

[43] J.J. Manyà, B. González, M. Azuara, G. Arner. Ultra-microporous adsorbents prepared from vine shoots-derived biochar with high CO2 uptake and CO2/N2 selectivity. Chemical Engineering Journal. 345 (2018) 631-9.

[44] J.F. Vivo-Vilches, A.F. Pérez-Cadenas, F.J. Maldonado-Hódar, F. Carrasco-Marín, R.P.V. Faria, A.M. Ribeiro, et al. Biogas upgrading by selective adsorption onto CO2 activated carbon from wood pellets. Journal of Environmental Chemical Engineering. 5 (2017) 1386-93.

[45] N. Álvarez-Gutiérrez, M.V. Gil, F. Rubiera, C. Pevida. Adsorption performance indicators for the CO2/CH4 separation: Application to biomass-based activated carbons. Fuel Processing Technology. 142 (2016) 361-9.

[46] Y.-J. Heo, S.-J. Park. A role of steam activation on CO2 capture and separation of narrow microporous carbons produced from cellulose fibers. Energy. 91 (2015) 142-50.

[47] A.S. Ello, L.K. de Souza, A. Trokourey, M. Jaroniec. Coconut shell-based microporous carbons for CO2 capture. Microporous and Mesoporous Materials. 180 (2013) 280-3.

[48] M. Thommes, K. Kaneko, A.V. Neimark, J.P. Olivier, F. Rodriguez-Reinoso, J. Rouquerol, et al. Physisorption of gases, with special reference to the evaluation of surface area and pore size distribution (IUPAC Technical Report). Pure and Applied Chemistry. 87 (2015) 1051.

[49] U.P. Agarwal, S.A. Ralph. FT-Raman Spectroscopy of Wood: Identifying Contributions of Lignin and Carbohydrate Polymers in the Spectrum of Black Spruce (Picea Mariana). Applied Spectroscopy. 51 (1997) 1648-55.

[50] A.C. Ferrari. Raman spectroscopy of graphene and graphite: Disorder, electron–phonon coupling, doping and nonadiabatic effects. Solid State Communications. 143 (2007) 47-57.

[51] A. Gomez-Martin, R. Chacartegui, J. Ramirez-Rico, J. Martinez-Fernandez. Performance improvement in olive stone's combustion from a previous carbonization transformation. Fuel. 228 (2018) 254-62.

[52] B. Cagnon, X. Py, A. Guillot, F. Stoeckli, G. Chambat. Contributions of hemicellulose, cellulose and lignin to the mass and the porous properties of chars and steam activated carbons from various lignocellulosic precursors. Bioresource Technology. 100 (2009) 292-8.

[53] D. Watkins, M. Nuruddin, M. Hosur, A. Tcherbi-Narteh, S. Jeelani. Extraction and characterization of lignin from different biomass resources. Journal of materials research and technology. 4 (2015) 26-32.

[54] J.Y. Yeo, B.L.F. Chin, J.K. Tan, Y.S. Loh. Comparative studies on the pyrolysis of cellulose, hemicellulose, and lignin based on combined kinetics. Journal of the Energy Institute. 92 (2019) 27-37.

[55] A. Gani, I. Naruse. Effect of cellulose and lignin content on pyrolysis and combustion characteristics for several types of biomass. Renewable Energy. 32 (2007) 649-61.

[56] P. Campos, A.Z. Miller, H. Knicker, M.F. Costa-Pereira, A. Merino, J.M. De la Rosa. Chemical, physical and morphological properties of biochars produced from agricultural

residues: Implications for their use as soil amendment. Waste Management. 105 (2020) 256-67.

[57] F. Rodriguez-Reinoso, M. Molina-Sabio, M. González. The use of steam and CO2 as activating agents in the preparation of activated carbons. Carbon. 33 (1995) 15-23.

[58] X. Zhou, H. Yi, X. Tang, H. Deng, H. Liu. Thermodynamics for the adsorption of SO2, NO and CO2 from flue gas on activated carbon fiber. Chemical Engineering Journal. 200 (2012) 399-404.

[59] N. Álvarez-Gutiérrez, M. Gil, F. Rubiera, C. Pevida. Adsorption performance indicators for the CO2/CH4 separation: Application to biomass-based activated carbons. Fuel Processing Technology. 142 (2016) 361-9.